Key Points:
- Velocities of positive and negative ions have been measured in the Enceladus plume using CAPS sensors
- Two distinct ion velocities are found, in agreement with fast gas and slow thermal emissions of neutrals
- Thermal negative ions are near stationary relative to Enceladus, implying a deceleration mechanism such as an ambipolar electric field

Correspondence to:
R. P. Haythornthwaite,
richard.haythornthwaite.18@ucl.ac.uk

Fast and Slow Water Ion Populations in the Enceladus Plume

R. P. Haythornthwaite[1,2] [iD], **A. J. Coates[1,2]** [iD], **G. H. Jones[1,2]** [iD], and **J. H. Waite[3]** [iD]

[1]Mullard Space Science Laboratory, Department of Space and Climate Physics, University College London, Dorking, UK, [2]Centre for Planetary Sciences at UCL/Birkbeck, London, UK, [3]Space Science Division, Southwest Research Institute, San Antonio, TX, USA

Abstract Ion velocities have been measured during the Enceladus E3 and E5 flybys using the Cassini Plasma Spectrometer (CAPS) instrument on the Cassini spacecraft. Data from three sensors in the CAPS instrument have been examined from two flybys that occurred during 2008. Positive ion measurements from the CAPS Ion Beam Spectrometer and Ion Mass Spectrometer have been used to measure positive ion velocities. The CAPS Electron Spectrometer has been used to complement the positive ion findings with measurements of negative ion velocities. Two velocities for the positive ions are found, with the fast ions (2.3–5.8 km/s) originating from the high-speed neutral gas emission and slow ions (0.2–2.2 km/s) associated with the low-speed thermal gas emission from Enceladus. Negative ions were found to be near stationary or northerly traveling, implying a deceleration mechanism within the plume. A tentative detection of fast negative ions was also recorded for one of the flybys. These findings will aid in future modeling of plume dynamics.

1. Introduction

Enceladus is the sixth largest moon of Saturn with an equatorial diameter of 513 km and was studied by the Cassini-Huygens mission to the Saturnian system. The investigation consisted of 22 targeted flybys of the moon between 2005 and 2015 that covered a variety of flyby velocities and geometries.

The most startling find of the flybys was the discovery of an outgassing plume emanating from around the moon's south pole (Dougherty et al., 2006). The plume's composition is dominated by water, confirmed by Ion Neutral Mass Spectrometer (INMS) (Waite et al., 2009), Ultraviolet Imaging Spectrograph (UVIS) (Hansen et al., 2006), and Cassini Plasma Spectrometer (CAPS) (Coates et al., 2010; Tokar et al., 2009) measurements. The plume was also found to originate from diffuse sources and collimated geyser-like jets. The jets were associated with a series of four fissures, commonly known as the "Tiger Stripes," that dominate the south polar terrain. From libration measurements and the jets, the existence of a 20–50 km deep global subsurface (Beuthe et al., 2016; Cadek et al., 2016) ocean was inferred, its presence also being necessary to supply the jets with material. The ocean itself is buried under a 20–30 km thick ice layer (Beuthe et al., 2016; Cadek et al., 2016). Around the south pole the ocean increases by 10 km in depth, while the ice thickness has a corresponding decrease, thinning out to between 2 and 5 km thick (Waite et al., 2019). The plume fly-throughs thereby allowed direct sampling of the ocean material providing an insight into the physics and chemistry present in the subsurface ocean.

It is well established that water is the major constituent in all three plume phases: dust, gas, and ions. The gas consists of neutral molecules with H_2O comprising up to 98% with other major species being CO_2, CH_4, NH_3, and H_2 (Waite et al., 2009, 2017, 2019). There are also hydrocarbons, alcohols, and nitriles detected at below 0.2% relative abundance to H_2O (Magee & Waite, 2017).

Various CAPS sensors have previously detected ions at Enceladus. CAPS Electron Spectrometer (ELS) has been used in the detection of negative ions, consisting of primarily water group ions (O^- and OH^-) (Coates et al., 2010) and clusters of these ions, likely in the form $(H_2O)_n$-OH^- or $(OH)_n$ (Postberg et al., 2018). These clusters were found to extend up to high masses (300–500 amu/q) with inferred densities in the plume between 0.1 and 50 cm^{-3}. Similarly, the CAPS Ion Mass Spectrometer (IMS) has complemented these findings with positive ion including H_2^+, water group ions (O^+, OH^+, H_2O^+, and H_3O^+) along with water dimer molecules (H_xO_2) (Tokar et al., 2009). The same study inferred that ion-neutral reactions in the plume

plasma as well as charge exchange between magnetospheric ions and plume neutral molecules are major sources of these ions. In situ photoionization has been shown to contribute to the ion population as well (Sakai et al., 2016). H_3O^+ as the dominant water group ion has also been shown through physical chemistry models of the plume (Fleshman et al., 2010), particle test models (Sakai et al., 2016) and in situ data from the INMS instrument (Cravens et al., 2009).

CAPS Ion Beam Spectrometer (IBS) data have been previously used to study the composition of Titan's atmosphere, reinforcing arguments on hydrocarbon detections made by INMS in addition to creating composition altitude profiles and quantifying their abundance (Crary et al., 2009; Westlake et al., 2014).

1.1. Particle Velocities in the Enceladus Plume

The plume gas emission has been shown to contain two distinct water components, a thermal population and a supersonic population (Teolis et al., 2017).

The thermal component arises from sublimation or through molecules interacting with fissure walls. The bulk velocities of these neutral water molecules in the plume have been estimated between 500 and 750 m/s, These measurements have been derived through various methods such as modeling (Smith et al., 2010; Tenishev et al., 2010), in situ measurements (Dong et al., 2011; Teolis et al., 2017), and UVIS measurements (Hansen et al., 2008).

The supersonic water population has been associated with driven fast gas emission from fissures. Some studies have found velocities from 1,200 up to 2,600 m/s (Hansen et al., 2011; Postberg et al., 2011). Through a combination of INMS and UVIS measurements, Teolis et al. (2017) suggested Mach numbers up to 10, corresponding to jet velocities of 6 km/s using a thermal velocity of 576 m/s. Other fitting attempts such as that performed by Yeoh et al. (2017) using INMS and UVIS data considering diffuse and jet sources, found velocities in excess of Mach 5 (1,500 m/s) caused by narrow jets at the vent represented best during the E5 flyby. Yeoh et al. (2017) found that Vents III, IV, and VI were the strongest influences during the E5 flyby. The model by Tenishev et al. (2014) fitted bulk velocities to the eight vents found by Spitale and Porco (2007), finding a range of velocities between 580 and 1,338 m/s.

There have also been attempts to model ion velocities inside the plume. Kriegel et al. (2011) modeled an ion bulk velocity less than 1 km/s inside the plume. Other modeling work by Sakai et al. (2016) modeled using velocities between 1 and 3 km/s.

2. Methodology

2.1. Instrumentation

In this paper we present data from all three of the CAPS sensors (Young et al., 2004). This includes data from the ELS, IMS, and IBS.

The CAPS ELS (Linder et al., 2013; Young et al., 2004) was designed to measure low-energy electrons between 0.55 and 26,600 eV/q across eight microchannel plate anodes, each with a field of view (FOV) of 5.2° in the azimuth and 20° in elevation. The energy resolution of the instrument was $\frac{\Delta E}{E} = 0.167$. These anodes combined create a total instantaneous FOV of 5.2° × 160° in azimuth and elevation respectively.

When particles enter the CAPS IMS they pass through a top hat electrostatic analyzer similar to ELS. Unlike ELS where the particles immediately impact the microchannel plates, IMS has a time-of-flight section. This time-of-flight section contains a linear electric field which aids in the separation of ions, neutrals, electrons and negative ions. CAPS IMS was designed to measure hot, diffuse magnetospheric plasma in addition to low-concentration ion species. The energy range of the instrument was 1–50,280 eV/q with an energy resolution of $\frac{\Delta E}{E} = 0.167$, and its FOV was similar to ELS with an instantaneous FOV of 8.3° × 160°.

The CAPS IBS was designed to determine the velocity of ion beams in the magnetosphere and the solar wind, in addition to studying Titan's upper atmosphere during flybys (Young et al., 2004). IBS is a curved-electrode electrostatic analyzer in contrast to the other CAPS sensors that are top hat analyzers. It consists of three apertures offset by 30° to each other in the view direction, each with a FOV of 1.5° × 150°. The apertures lead to spherical electrodes that extend 178° from the aperture which the particles pass between before impacting on channel-electron multipliers (CEMs). The energy range of IBS is similar to IMS at 1–49,800 eV/q but its energy resolution of $\frac{\Delta E}{E} = 0.014$ is more than an order of magnitude higher than IMS due to its longer curved electrode.
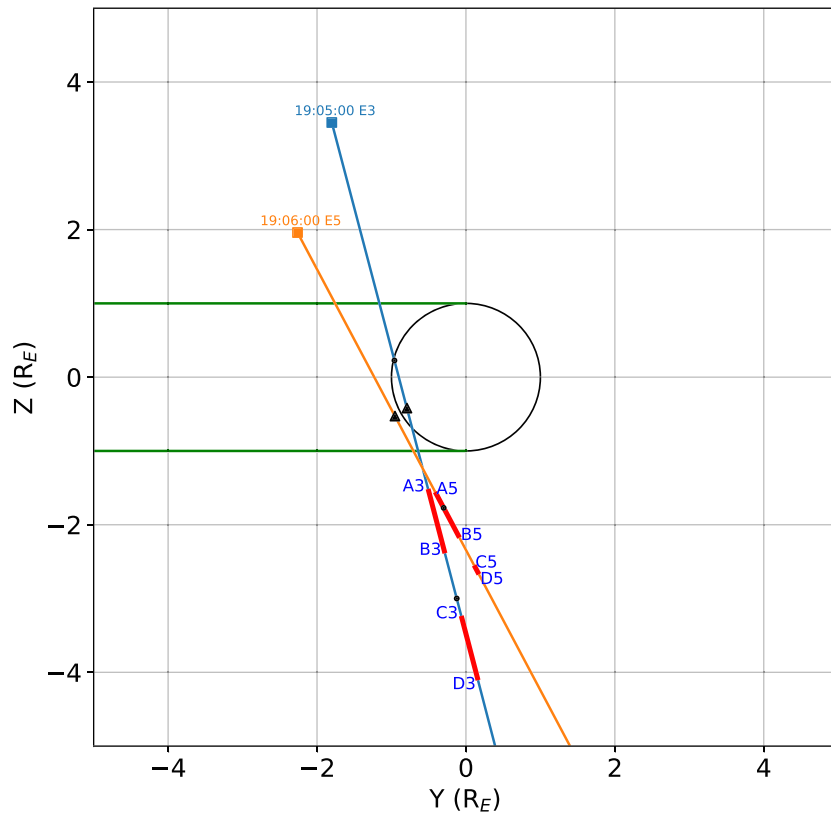
Figure 1. The Cassini trajectory in the *YZ* plane, during the E3 and E5 flybys. Negative *Y* is in the direction of the corotation of magnetospheric plasma. The highlighted red areas of the trajectories between the labels A#-B# and C#-D# where # is 3 or 5 correspond to the E3 and E5 flybys, respectively, are the regions where the low-energy peak occurs in the energy spectrograms. Similar labels can be found in all subsequent figures. The squares indicate an arbitrary start location to help demonstrate the north-south direction that Cassini traveled in, the black triangle indicates the location of closest approach, while the dots indicate Cassini locations at 1 min intervals. The geometric corotational wake of Enceladus is indicated by the green lines.

2.2. Methods

In a plasma environment where the spacecraft velocity with respect to the bulk flow is very large, temperatures are low and the kinetic energy in the relative frame is $\frac{1}{2}mv_{sc}^2$, the plasma is measured by CAPS as a highly directed ion population traveling at Cassini velocities. This means that the detected energy/charge of the particles can be related to the mass/charge of the particle and by applying this approximation an eV/q spectrum can be converted to an amu/q spectrum. As seen in equation (1) the conversion is affected by both spacecraft velocity and the spacecraft potential. The potential energy shift must be performed in phase space density to satisfy Liouville's theorem (e.g., Lewis et al., 2008), which states that the phase space density of a distribution must be conserved along the trajectory of the system. Furthermore, there is a charge dependence on the energy and mass values ($Q = +1$ for positive ions, -1 for electrons and negative ions), therefore a determination of mass rather than mass/charge must include the presumption of a singularly charged ion.

$$\frac{m}{q} = \frac{2}{q(v_{sc} - v_i)^2}(E + Q\Phi_{sc}) \tag{1}$$

This technique has been previously used at Titan (Coates et al., 2007; Crary et al., 2009; Desai et al., 2017) and at Enceladus (Coates et al., 2010; Hill et al., 2012; Jones et al., 2009). The along-track ion velocity term v_i has not previously been accounted for at Enceladus but has been accounted for at Titan (Crary et al., 2009; Westlake et al., 2014), the addition of this term is explained in section 3.1.2.

Using ELS as a negative ion mass spectrometer further treatment of the data is required. This is due to electron counts from various populations such as magnetospheric electrons and photoelectron peaks (Coates et al., 2013; Taylor et al., 2018). As stated previously, the ions appear as a highly directed supersonic population traveling at Cassini's velocity in ELS, this means the negative ions only appear in the central anodes of
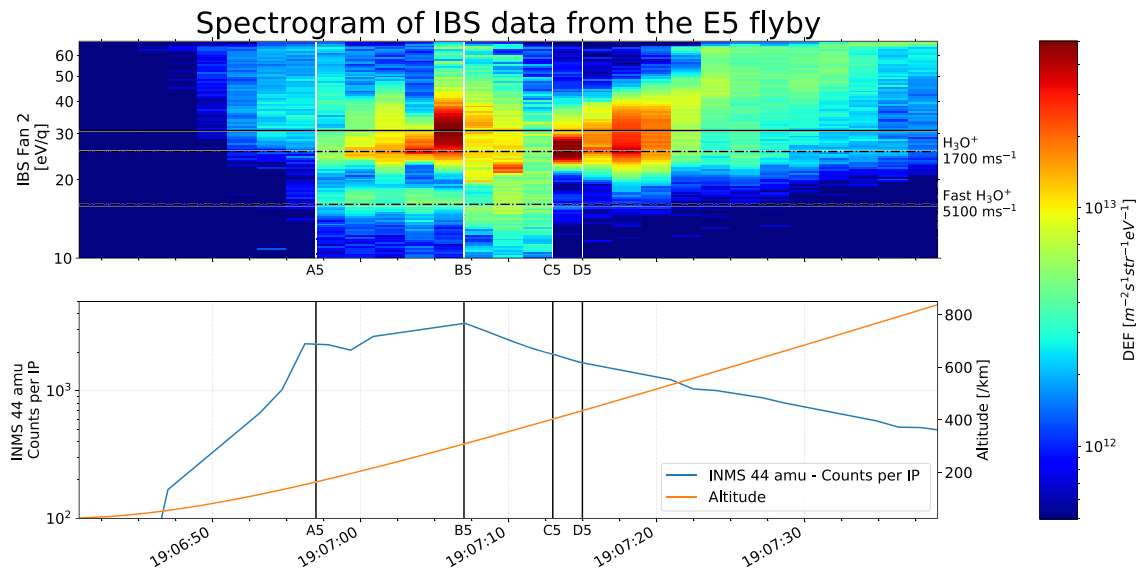
Figure 2. The first panel is an energy spectrogram from IBS Fan 2 during the E5 flyby. Horizontal lines demonstrate the energy location of the presumed major water ion H_3O^+, with the solid line displaying the energy location when assumed to be stationary in the plume frame, while the dot-dashed lines display the molecules' positions with an along-track velocity away from Cassini and a constant spacecraft potential taken into account. Fast H_3O^+ fits a velocity of 5.1 km/s, while the main H_3O^+ population fits a velocity of 1.7 km/s. The second panel plots 44 amu neutral counts/IP from the INMS instrument; see Perry et al. (2015) for details. In addition, Cassini's altitude above the Enceladus surface is plotted.

the sensor. The central anodes or ram anodes were typically the fourth and fifth anodes during encounters due to the spacecraft attitude and CAPS being actuated so that Cassini's velocity vector was between the two anodes. To reduce the possibility that the detected peak is associated with an electron population an assumed background isotropic electron distribution was found by averaging over the nonram anodes (Anodes 1–3 and 6–8) (Desai et al., 2017; Wellbrock et al., 2013). This background was then subtracted off the ram anodes to isolate the negative ion signal. The remaining peaks in the spectrograms after this background removal are interpreted as negative ion peaks.

3. Results

3.1. E5 Flyby

E5 was a targeted Enceladus flyby that took place in October 2008. It was the fastest flyby at 17.7 km/s and the nearest with a closest approach at 25 km. The north-south trajectory of the flyby, as seen in Figure 1, meant it followed along the plume motion as the emissions move southward away from Enceladus.

3.1.1. E5 Positive Water Ions

Positive ions during the E5 flyby have been previously studied by Tokar et al. (2009) using CAPS-IMS.

An energy-time spectrogram displaying data from Fans 1 and 2 of CAPS IBS during the E5 flyby can be seen in Figure 2. The main peak seen in the spectrogram can be associated with the dominant ion species present in the plume, the water group ion H_3O^+. The secondary lower energy peak that occurs at 19:06:55 is the subject of interest of this paper. The background ions drop out occurs at 19:06:37, along with a peak that decreases in energy from 19:06:45 to 19:06:55. As noted by Tokar et al. (2009), this peak is associated with H_3O^+ being formed in the plume that is gradually accelerated and dragged into the magnetospheric wake.

At the B5 location in Figure 2 the energy peak structure can be seen to break down when Cassini is due south of Enceladus. As confirmed by INMS measurements seen in the lower panel of Figure 2 Cassini is in the densest region of the plume. The sweeps between B5 and C5 lack clear peak structure, this could be due to masking from dust grain impacts in the instrument creating anomalous peaks, as this is when Cassini traversed a more active (Yeoh et al., 2017) and higher dust-to-gas ratio region (Hedman et al., 2018). Another possible cause of the peak structure disruption in the B5-C5 energy sweeps could be the time-aliasing of the instrument in the highly dynamic plume environment. Despite the possible instrument effects, the low-energy peak appears to shift to a lower energy in the first sweep after B5, this could be indicative of an increase in ion velocity due to Cassini passing through the middle of a high-velocity jet.

Table 1
The Velocity Ranges of Positive and Negative Ions in Meter per Second for the Two Enceladus Flybys Examined

	E3	E5
Slow H_3O^+	[200, 2,000]	[1,400, 2,200]
Fast H_3O^+	[2,300, 4,800]	[4,550, 5,800]
Slow OH^-	[−1800, −300]	[−1,600, 450]
Fast OH^-	—	[3,000, 5,000]

Note. The ranges result from spacecraft potential discrepancies and the energy resolution of the CAPS sensors. E3 H_3O^+ velocities are calculated from IMS data, while E5 H_3O^+ velocities are calculated from IBS data. ELS is used for both E3 and E5 in the OH^- ion velocity determination.

The horizontal lines in Figure 2 indicate energies of various molecules with different characteristics, the energies of which have been determined using equation (1). We note that previous spacecraft potential discrepancies found between CAPS and the Radio and Plasma Wave Langmuir probe (LP) range between 0.5 and −2 V (Coates et al., 2007; Desai et al., 2017; Schippers et al., 2009) and that the LP potential varies from −0.43 to −1.27 V during the E5 encounter. However, if a positive spacecraft potential existed due to discrepancies, positive ion energies would be reduced. If spacecraft potential is solely considered to explain the low-energy peak seen in Figure 2, a positive voltage of +5 V would be needed to explain the H_3O^+ peak. This would be an order of magnitude larger than previous reported discrepancies and would affect both energy peaks in a similar fashion, therefore this explanation is unlikely. Furthermore if spacecraft potential is solely considered, the energy offset would also affect CAPS ELS data by increasing the negative ion energies but this effect is not detected.

This requires another mechanism to explain the low-energy peak seen in the plume.

3.1.2. Ion Velocities

If a velocity component exists along Cassini's trajectory, it affects the measured energy/charge ratio of the particles. Previously used mass-energy conversions for CAPS have considered ions at rest relative to Enceladus implying that in the Cassini frame (Coates et al., 2010; Tokar et al., 2009), the particles are moving toward CAPS at the spacecraft ram velocity. If a nonzero velocity exists in the Enceladus frame there can exist an ion velocity component along the Cassini trajectory. A velocity component pointing away from Cassini would result in the reduction of the relative velocity between Cassini and the ions, adding an extra term in equation (1).

Reducing the relative velocity of the molecules results in the molecules appearing at lower energies. As seen in Figure 2, correcting with a constant spacecraft potential and applying an ion velocity of ∼1,700 m/s results in the major peak in the spectrogram aligning with the expected H_3O^+ peak. Applying the same method to the lower energy peak requires an ion velocity of ∼5,100 m/s.

Table 1 contains the ranges of velocities that could account for the peaks seen in the CAPS sensors. This has been applied across the entire plume encounter which is likely incorrect as variations in the velocity would be expected during the encounter, this likely effect can be seen when the lower peak at 19:07:07 shifts to lower energies. However determining the velocity on a sweep-by-sweep basis has not been attempted, due to a lack of detailed information on the spacecraft potential at the same temporal resolution.

3.1.3. Peak-Source Correspondence

Jones et al. (2009) found correspondence between dust peaks seen in CAPS ELS and IMS spectrograms and the reported jet sources in the fissures (Spitale & Porco, 2007). By applying the vent findings from Jones et al. (2009) we find that the start of the lower energy peak at 19:06:57 matches the E5i1 peak (see Jones et al., 2009), which was associated with Vent V. This vent was assigned a bulk velocity of 1,030 m/s by Tenishev et al. (2014). However, this assignment does not concur with the results of Yeoh et al. (2017), they find Vent III to be the major source. Assuming the Vent V assignment is correct it implies the ion velocity is 570 m/s higher than the neutral bulk velocity but this still lies in the range reported by Hansen et al. (2011). Furthermore plume ions could be accelerated outward by electric fields in the plume (Farrell et al., 2010; Jones et al., 2009; Sakai et al., 2016), possibly up to several kilometers per second.
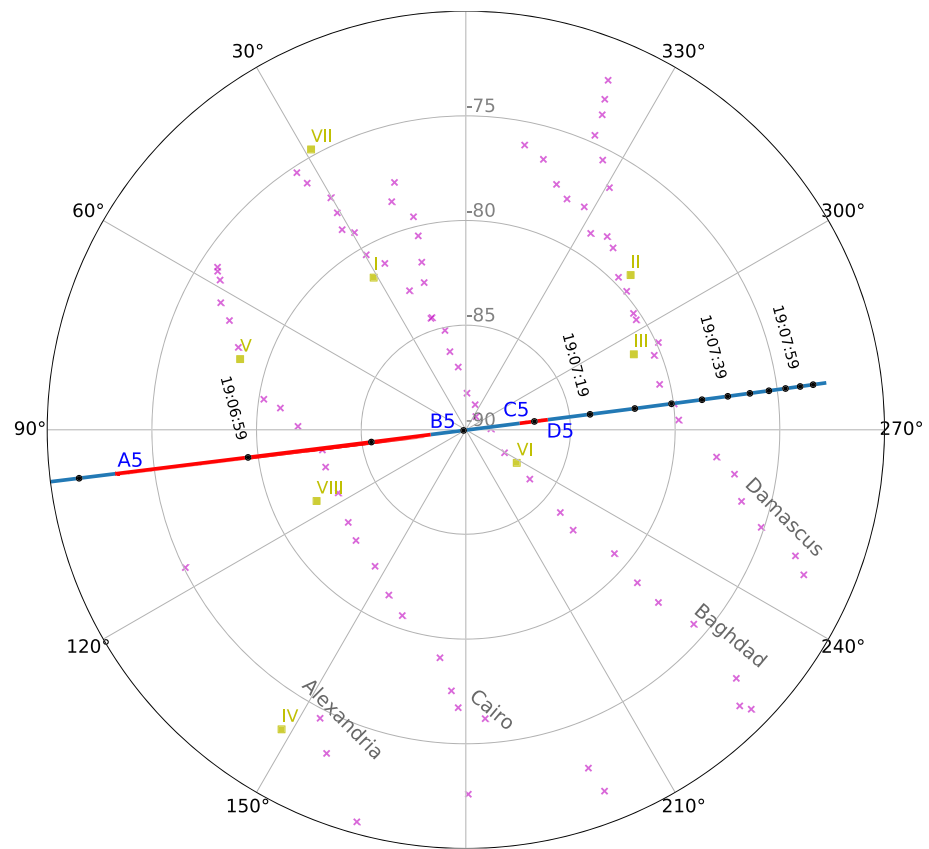
Figure 3. Diagram of the E5 flyby surface track over the south polar fissures. Black dots on the track are 5 s markers. Yellow squares indicate the vent locations as identified by Spitale and Porco (2007), while pink crosses indicate the jet sources from Porco et al. (2014). The red regions of the surface track are the times where the low-energy peak can be seen (19:06:55–19:07:07, 19:07:13–19:07:15).

There is also the possibility that the associated source is not one of the earlier reported vents but one of the 98 jets later identified by Porco et al. (2014). Teolis et al. (2017) studied three flybys in 2010–2011 that were low altitude horizontal flybys. Using optical and ultraviolet images, as well as 3-D modeling, they constrained the magnitudes and velocities of the jets detected using high spatial resolution measurements from INMS. They find large variability between flybys and along the fissures along with a mixture of low- and high-velocity gas emissions, with gas being accelerated up to Mach 10. In their modeling they apply the 98 jets from Porco et al. (2014) and find that some of the jets correspond well with high velocities seen in INMS. Contributions from 98 jets is not considered in this work due to the lack of spatial information in the data, possible mixing from multiple jets and temporal variability.

In Figure 3, a break in the occurrence of the peak can be seen corresponding to the interval 19:07:07–19:07:13. This interval also corresponds to Cassini's passage over the south pole and the Baghdad sulcus. 19:07:09–19:07:13 was identified as a positive nanograin peak by Jones et al. (2009), originating from the nearby Vent VI. This leads to the interpretation of charged nanograins or neutral dust affecting IBS during this timeframe obscuring the peak structure.

A similar effect does occur at the Cairo sulcus crossing but not at the same intensity. The main water peak broadens and the lower peak is weakened during the 19:07:01–19:07:03 IBS sweep. The lower intensity could be due to a reduced dust-gas ratio at the Cairo sulcus compared to Baghdad (Hedman et al., 2018), it could also be due to less active jets (Yeoh et al., 2017).

3.1.4. E5 Negative Water Ions

As described in section 2.2, the CAPS ELS can be used as an anion spectrometer when viewing a highly directed negative ion population. Negative ions were previously studied in the Enceladus plume by Coates et al. (2010); Coates et al. (2010). During these studies the negative ions were assumed to be stationary relative to Enceladus.
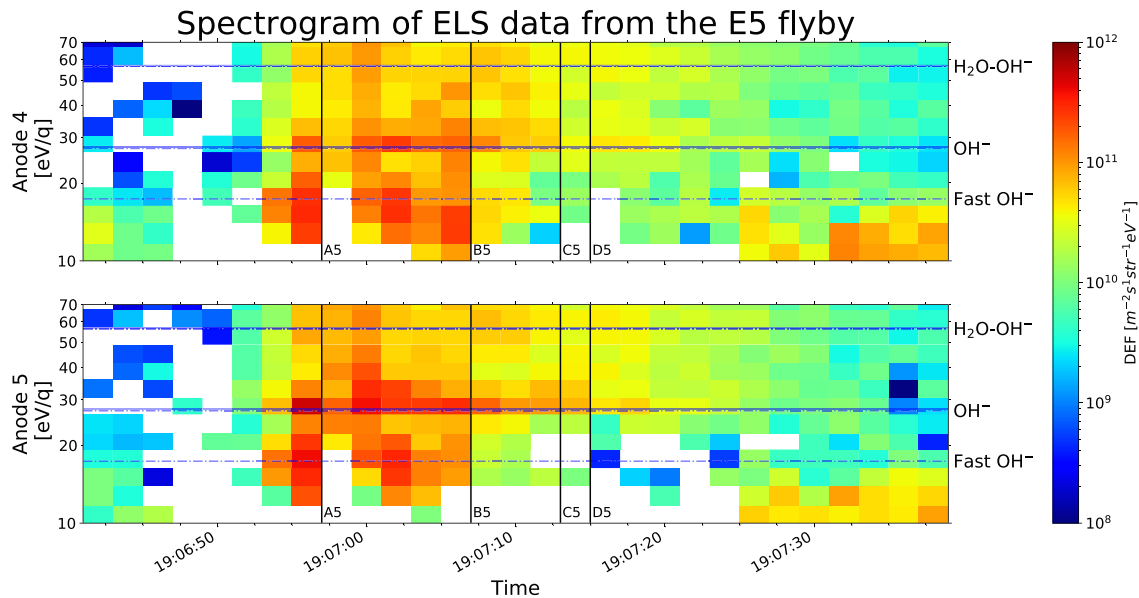
Figure 4. Energy spectrogram of the ELS ram anodes (4 and 5) during the E5 flyby. An isotropic electron background calculated from the mean of the nonram anodes has been removed. The lines represent energies of various molecules, dot-dashed lines represent the same energies with spacecraft potential and ion velocity corrections applied.

Applying similar methods to that performed with the positive ions, velocities of negative ions during the E5 flyby are found using ELS data, a spectrogram of ELS data can be seen in Figure 4. During E5 flyby a range of velocities are found for the OH⁻ ions, between −1,600 and 450 m/s and therefore agree with the assumption of stationary or nearly stationary ions. This negative ion population is likely associated with the slower neutral population due to its low velocity.

A tentative low-energy peak appears once the isotropic electron background is removed. As the peak exists at the upper energy range of the electron energies the detection of a low-energy negative ion peak is tentative. If this low-energy peak is associated with fast moving OH⁻ ions, its resulting velocity would be between 3,000 and 5,000 m/s. Similar to the positive ions this peak could be associated with the fast neutral population. The velocities of the negative ions appear to be lower than the positive ions, implying a deceleration of the negative water ions once the neutral water molecules are ionized

3.2. E3 Flyby

As seen in Figure 1, E3 was another targeted Enceladus flyby that took place before E5 in March 2008, also having a similarly inclined north-south trajectory with a comparable velocity of 14.4 km/s.

3.2.1. E3 Low-Energy Peak

During the E3 flyby CAPS IBS was operating in a high energy mode, resulting in ions below 80 eV not being detected, therefore it cannot be used in this study. However another sensor in the CAPS instrument package can be used, the IMS. During the E5 flyby no rammed ion peak occurs consistently across consecutive energy sweeps in the CAPS IMS instrument. A possible cause are dust particles or neutral molecules impacting CAPS that proceed to vaporize and ionize in the instrument, this could cause anomalous energy peaks that mask the rammed ion peak. This possibility would be consistent with the higher velocity of E5 compared to E3, along with the increased neutral gas density (Perry et al., 2015) and dust density (Teolis et al., 2010) of E5 compared to E3.

Unlike E5, CAPS IMS observed positive ions during the E3 flyby and as seen in the IMS energy-time spectrogram in Figure 5, three rammed ion peaks occur inside the plume. These peaks have been previously studied by Tokar et al. (2009), with the peaks being attributed to O^+, H_3O^+ and a water dimer ion.

The low-energy peak appears after energy of the main water group peak becomes constant, at around 19:06:30. The lower peak also appears in conjunction with the emergence of the dimer peak. The timing of the low-energy peak is similar to the peak emergence in the IBS data for the E5 flyby.
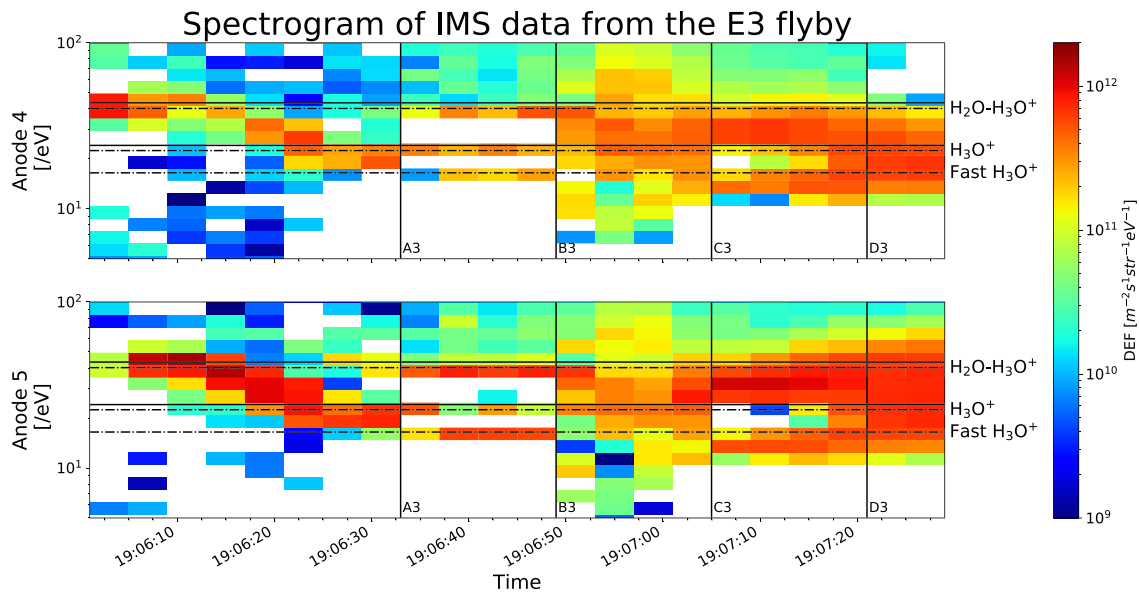
Figure 5. Energy spectrogram of the IMS ram anodes (4 and 5) during the E3 flyby. Horizontal lines indicate energy locations of various molecules, solid lines indicate the location of an entirely stagnated flow without corrections, while the dot-dashed lines indicate the locations with spacecraft potential and an ion velocity corrections applied.

Examining the energy locations of molecules, a faster water group ion explains the presence of the low-energy peak. The spacecraft potential during the E3 flyby is approximately −3 to −4 V, as measured by the Radio and Plasma Wave Langumir probe, shifting the positive ions to higher energies. If this effect is taken in isolation, then the energy locations of the detected peaks would not be associated with water group ions. Therefore ion velocities are taken into account, to reduce the energy of H_3O^+ to align it the slow population with the major peak and the fast population with the low-energy peak. The combination of these corrections leads to (1) H_3O^+ and the water dimer are slowly moving ions, (2) the energy of slow moving O^+ is between the two lower peaks, and (3) the lower peak must be associated with a faster water group ion population.
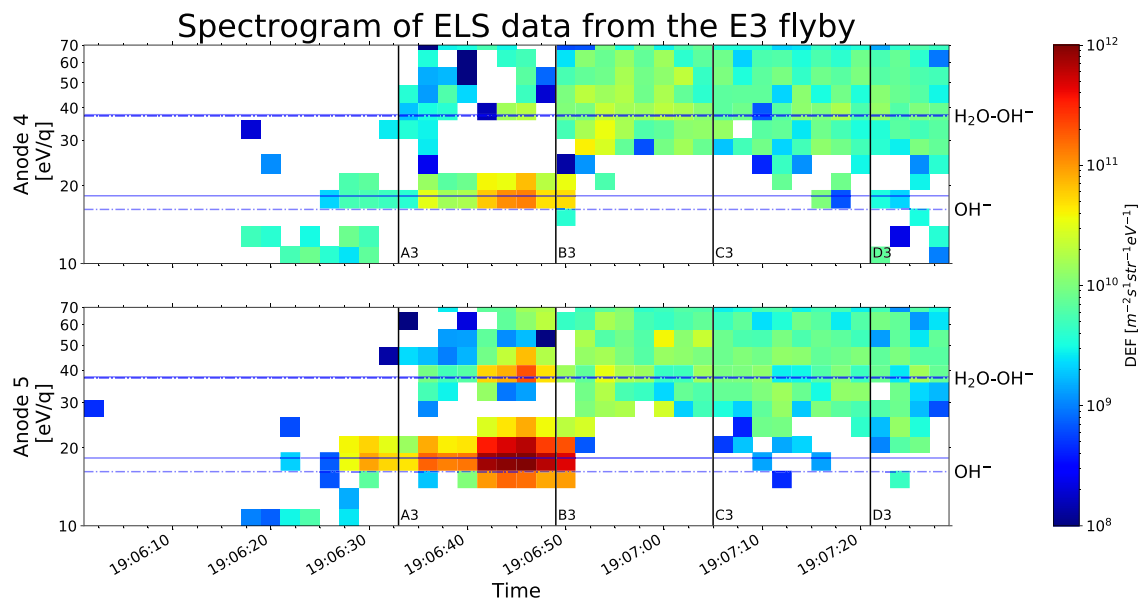

Figure 6. Spectrogram using ELS data from the E3 flyby, with similar annotations to Figure 4.

3.2.2. E3 Negative Water Ions

Similar to E5 negative ions are seen during the E3 flyby. The spectrogram for the E3 flyby can be seen in Figure 6.

The lack of a negative ion peak associated with a faster water ion group during the E3 flyby could be due to several factors. First, the peak could be obscured by the electron background present in the plume. Second, the production rates of negative ions are low compared to positive ions, therefore the peak intensity may be too low to register.

4. Discussion

The low-energy peak is only seen in the E3 and E5 north-south directed flybys and not the later flybys E7, E17 and E18 which traversed horizontally across the plume . This implies that the geometry of the flyby is significant and supports the interpretation of a highly directed fast water ion population.

The variation of measured ion velocities between the flybys can be attributed to the different geometry of the flybys. The Y velocity component of the E5 flyby was just over 50% of the Z velocity component, while at E3 it was just under 25%. This has been previously noted in modeling work by Sakai et al. (2016). This difference in the relative components could explain the velocity discrepancies as CAPS sensors can only measure along-track velocities using the applied method.

The generation of the two water group positive ion populations is likely through charge exchange (Omidi et al., 2012; Sakai et al., 2016; Tokar et al., 2009). Charge exchange is associated with fast moving ions interacting with slow moving neutrals. There is only a small amount of energy transfer to the newly created ion during charge exchange, meaning these ions retain similar kinetic energies to their neutral progenitors. This implies that the two ion populations can be created from two neutral populations with different velocities.

4.1. EM Fields

The magnetic field within the plume is largely $-Z$ directed with perturbations due to the plume material (Dougherty et al., 2006). The presence of the magnetic field causes newly created ions to be picked up and gyrate away from Saturn. As magnetic fields cannot do work on particles, the energy difference between the positive and negative ions requires other forces to be present. The origin of these forces could be an ambipolar electric field present within the plume. These fields have been modeled in several studies (Omidi et al., 2012; Sakai et al., 2016). Sakai et al. (2016) proposed an electric field strength of -10 μV/m in the Z axis, a field of this magnitude would both accelerate positive ions southward and decelerate negative ions, causing a large velocity component along Cassini's track during the nouth-south directed E3 and E5 flybys. The longer lifetimes of positive ions compared with negative ions could result in stronger acceleration effects.

Negative ions were presumed to be stationary relative to Enceladus due to the local production and short lifetimes of the molecules. However during the studied flybys a range of valid ion velocities exist (see Table 1), where the negative ions would be detected in the same energy bin of ELS. For example during E5 the maximum possible OH^- ion velocity was 300 m/s, the deceleration caused by an electric field of -10 μV/m would be approximately 60 m/s^2, requiring only 2.5 s to achieve this deceleration. Comparing to the proposed lifetimes in Coates et al. (2010) of 6 s for H^-, this deceleration appears reasonable. Furthermore, OH^- lifetimes are likely higher than that of H^- due to their higher electron affinity providing greater stability, thereby allowing greater deceleration. This could explain the velocities of negative ions during E3, with the required lifetime being 15 s.

4.2. Other Possibilities

Another possibility could be doubly charged ions, resulting in a candidate molecule of 24 amu. Although there are candidate molecules in this mass range which could form doubly charged particles, they are unlikely in the plume due to the required energetics and their lifetimes being on the order of a few seconds or less (Thissen et al., 2011).

The lower peak being associated with N^+ ions is possible but unlikely. Enceladus has previously been shown to be a major source of nitrogen in Saturn's magnetosphere (H. Smith et al., 2007; H. T. Smith et al., 2008). However this explanation would require the water peak to be associated with OH^+ and multiple reactions from a neutral ammonia source. Given that H_3O^+ is currently considered as the dominant ion and multiple reactions are unlikely, this possibility is not considered further.

5. Summary and Conclusions

Ion velocities have been measured in the Enceladus plume, with both fast and slow water ion populations being found. Data from all three CAPS sensors have been utilized across two flybys that occurred in 2008, CAPS IMS data were used during the E3 flyby, while IBS data were examined during the E5 flyby. Two separate positive water ion velocity distributions were found, originating from the two neutral populations within the plume: the slow thermalized emission and the fast gas emission (Teolis et al., 2017). Through processes such as charge exchange these neutral water molecules become ionized and retain their kinetic energy, generating two distinct ion energy peaks within the plume.

Negative ions were also analyzed using CAPS ELS data, with ion velocities nearly stagnant in the plume but decelerated compared to the neutral molecules/positive ions. These findings add to the discussion over the presence of a southwardly directed ambipolar electric field in the plume, generated through plasma pressure or negative grains (Jones et al., 2009; Sakai et al., 2016).

References

Beuthe, M., Rivoldini, A., & Trinh, A. (2016). Enceladus's and Dione's floating ice shells supported by minimum stress isostasy. *Geophysical Research Letters*, *43*, 10,088–10,096. https://doi.org/10.1002/2016GL070650

Cadek, O., Tobie, G., Van Hoolst, T., Massé, M., Choblet, G., Lefévre, A., et al. (2016). Enceladus's internal ocean and ice shell constrained from Cassini gravity, shape, and libration data. *Geophysical Research Letters*, *43*, 5653–5660. https://doi.org/10.1002/2016GL068634

Coates, A. J., Crary, F. J., Lewis, G. R., Young, D. T., Waite Jr., J. H., & Sittler, E. C. Jr. (2007). Discovery of heavy negative ions in Titan's ionosphere. *Geophysical Research Letters*, *34*, L22103. https://doi.org/10.1029/2007GL030978

Coates, A. J., Jones, G. H., Lewis, G. R., Wellbrock, A. A., Young, D. T., Crary, F. J., et al. (2010). Negative ions in the Enceladus plume. *Icarus*, *206*(2), 618–622. Retrieved from http://www.sciencedirect.com/science/article/pii/S0019103509003030 (Cassini at Saturn) https://doi.org/10.1016/j.icarus.2009.07.013

Coates, A. J., Wellbrock, A., Jones, G. H., Waite, J. H., Schippers, P., Thomsen, M. F., et al. (2013). Photoelectrons in the Enceladus plume. *Journal of Geophysical Research: Space Physics*, *118*, 5099–5108. https://doi.org/10.1002/jgra.50495

Coates, A. J., Wellbrock, A., Lewis, G. R., Jones, G. H., Young, D. T., Crary, F. J., et al. (2010). Negative ions at Titan and Enceladus: Recent results. *Faraday Discuss*, *147*, 293–305. https://doi.org/10.1039/C004700G

Crary, F. J., Magee, B. A., Mandt, K., Waite, J. H., Westlake, J., & Young, D. T. (2009). Heavy ions, temperatures and winds in Titan's ionosphere: Combined Cassini CAPS and INMS observations. *Planetary and Space Science*, *57*(14), 1847–1856. Retrieved from http://www.sciencedirect.com/science/article/pii/S0032063309002682, https://doi.org/10.1016/j.pss.2009.09.006

Cravens, T. E., McNutt Jr., R. L., Waite Jr., J. H., Robertson, I. P., Luhmann, J. G., Kasprzak, W., & Ip, W. H. (2009). Plume ionosphere of Enceladus as seen by the Cassini ion and neutral mass spectrometer. *Geophysical Research Letters*, *36*, L08106. https://doi.org/10.1029/2009GL037811

Desai, R. T., Coates, A. J., Wellbrock, A., Vuitton, V., Crary, F. J., González-Caniulef, D., et al. (2017). Carbon chain anions and the growth of complex organic molecules in Titan's ionosphere. *The Astrophysical Journal*, *844*(2), L18. https://doi.org/10.3847/2041-8213/aa7851

Dong, Y., Hill, T. W., Teolis, B. D., Magee, B. A., & Waite, J. H. (2011). The water vapor plumes of Enceladus. *Journal of Geophysical Research*, *116*, A10204. https://doi.org/10.1029/2011JA016693

Dougherty, M. K., Khurana, K. K., Neubauer, F. M., Russell, C. T., Saur, J., Leisner, J. S., & Burton, M. E. (2006). Identification of a dynamic atmosphere at Enceladus with the Cassini magnetometer. *Science*, *311*(5766), 1406–1409. https://doi.org/10.1126/science.1120985

Farrell, W. M., Kurth, W. S., Tokar, R. L., Wahlund, J. E., Gurnett, D. A., Wang, Z., et al. (2010). Modification of the plasma in the near-vicinity of Enceladus by the enveloping dust. *Geophysical Research Letters*, *37*, L20202. https://doi.org/10.1029/2010GL044768

Fleshman, B. L., Delamere, P. A., & Bagenal, F. (2010). Modeling the Enceladus plume-plasma interaction. *Geophysical Research Letters*, *37*, L03202. https://doi.org/10.1029/2009GL041613

Hansen, C. J., Esposito, L., Stewart, A. I. F., Colwell, J., Hendrix, A., Pryor, W., et al. (2006). Enceladus' water vapor plume. *Science*, *311*(5766), 1422–1425. Retrieved from https://science.sciencemag.org/content/311/5766/1422, https://doi.org/10.1126/science.1121254

Hansen, C. J., Esposito, L., Stewart, A. I. F., Meinke, B., Wallis, B., Colwell, J. E., et al. (2008). Water vapour jets inside the plume of gas leaving Enceladus. *Nature*, *456*(7221), 477–479. https://doi.org/10.1038/nature07542

Hansen, C. J., Shemansky, D. E., Esposito, L. W., Stewart, A. I. F., Lewis, B. R., Colwell, J. E., et al. (2011). The composition and structure of the Enceladus plume. *Geophysical Research Letters*, *38*, L11202. https://doi.org/10.1029/2011GL047415

Hedman, M. M., Dhingra, D., Nicholson, P. D., Hansen, C. J., Portyankina, G., Ye, S., & Dong, Y. (2018). Spatial variations in the dust-to-gas ratio of Enceladus' plume. *Icarus*, *305*, 123–138. https://doi.org/10.1016/j.icarus.2018.01.006

Hill, T. W., Thomsen, M. F., Tokar, R. L., Coates, A. J., Lewis, G. R., Young, D. T., et al. (2012). Charged nanograins in the Enceladus plume. *Journal of Geophysical Research*, *117*, A05209. https://doi.org/10.1029/2011JA017218

Jones, G. H., Arridge, C. S., Coates, A. J., Lewis, G. R., Kanani, S., Wellbrock, A., et al. (2009). Fine jet structure of electrically charged grains in Enceladus' plume. *Geophysical Research Letters*, *36*, L16204. https://doi.org/10.1029/2009GL038284

Kriegel, H., Simon, S., Motschmann, U., Saur, J., Neubauer, F. M., Persoon, A. M., et al. (2011). Influence of negatively charged plume grains on the structure of Enceladus' Alfvén wings: Hybrid simulations versus Cassini Magnetometer data. *Journal of Geophysical Research*, *116*, A10223. https://doi.org/10.1029/2011JA016842

Lewis, G. R., André, N., Arridge, C. S., Coates, A. J., Gilbert, L. K., Linder, D. R., & Rymer, A. M. (2008). Derivation of density and temperature from the Cassini-Huygens CAPS electron spectrometer. *Planetary and Space Science*, *56*(7), 901–912. https://doi.org/10.1016/j.pss.2007.12.017

Linder, D. R., Coates, A. J., Woodliffe, R. D., Alsop, C., Johnstone, A. D., Grande, M., et al. (2013). The Cassini caps electron spectrometer. In *Measurement techniques in space plasmas: Particles* (pp. 257–262). Washington, DC: American Geophysical Union. https://doi.org/10.1029/GM102p0257

Magee, B. A., & Waite, J. H. (2017). Neutral gas composition of Enceladus' plume—Model parameter insights from Cassini-INMS. In *Lunar and planetary science conference* (pp. 2974).

Omidi, N., Tokar, R. L., Averkamp, T., Gurnett, D. A., Kurth, W. S., & Wang, Z. (2012). Flow stagnation at Enceladus: The effects of neutral gas and charged dust. *Journal of Geophysical Research*, *117*, A06230. https://doi.org/10.1029/2011JA017488

Perry, M. E., Teolis, B. D., Hurley, D. M., Magee, B. A., Waite, J. H., Brockwell, T. G., et al. (2015). Cassini INMS measurements of Enceladus plume density. *Icarus*, *257*, 139–162. https://doi.org/10.1016/j.icarus.2015.04.037

Porco, C., DiNino, D., & Nimmo, F. (2014). How the geysers, tidal stresses, and thermal emission across the south polar terrain of Enceladus are related. *The Astronomical Journal*, *148*(3), 45. https://doi.org/10.1088/0004-6256/148/3/45

Postberg, F., Clark, R. N., Hansen, C. J., Coates, A. J., Dalle Ore, C. M., Scipioni, F., et al. (2018). Plume and surface composition of Enceladus. In P. M. Schenk, R. N. Clark, C. J. A. Howett, A. J. Verbiscer, & J. Hunter Waite (Eds.), *Enceladus and the icy moons of Saturn* (Vol. 475, pp. 129). Tucson: University of Arizona Press. https://doi.org/10.2458/azu_uapress_9780816537075-ch007

Postberg, F., Schmidt, J., Hillier, J., Kempf, S., & Srama, R. (2011). A salt-water reservoir as the source of a compositionally stratified plume on Enceladus. *Nature*, *474*, 620 EP. https://doi.org/10.1038/nature10175

Sakai, S., Cravens, T. E., Omidi, N., Perry, M. E., & Waite, J. H. (2016). Ion energy distributions and densities in the plume of Enceladus. *Planetary and Space Science*, *130*, 60–79. Retrieved from http://www.sciencedirect.com/science/article/pii/S0032063316301295 (Atmospheres, Magnetospheres and Surfaces of the outer planets, their satellites and ring systems: Part XI).

Schippers, P., André, N., Johnson, R. E., Blanc, M., Dandouras, I., Coates, A. J., et al. (2009). Identification of photoelectron energy peaks in Saturn's inner neutral torus. *Journal of Geophysical Research*, *114*, A12212. https://doi.org/10.1029/2009JA014368

Smith, H. T., Johnson, R. E., Perry, M. E., Mitchell, D. G., McNutt, R. L., & Young, D. T. (2010). Enceladus plume variability and the neutral gas densities in Saturn's magnetosphere. *Journal of Geophysical Research*, *115*, A10252. https://doi.org/10.1029/2009JA015184

Smith, H. T., Johnson, R. E., Sittler, E. C., Shappirio, D., Tucker, O. J., et al. (2007). Enceladus: The likely dominant nitrogen source in Saturn's magnetosphere. *Icarus*, *188*(2), 356–366. Retrieved from http://www.sciencedirect.com/science/article/pii/S0019103506004556, https://doi.org/10.1016/j.icarus.2006.12.007

Smith, H. T., Shappirio, M., Johnson, R. E., Reisenfeld, D., Sittler, E. C., Crary, F. J., et al. (2008). Enceladus: A potential source of ammonia products and molecular nitrogen for Saturn's magnetosphere. *Journal of Geophysical Research*, *113*, A11206. https://doi.org/10.1029/2008JA013352

Spitale, J. N., & Porco, C. C. (2007). Association of the jets of Enceladus with the warmest regions on its south-polar fractures. *Nature*, *449*, 695–697.

Taylor, S. A., Coates, A. J., Jones, G. H., Wellbrock, A., Fazakerley, A. N., Desai, R. T., et al. (2018). Modeling, analysis, and interpretation of photoelectron energy spectra at Enceladus observed by Cassini. *Journal of Geophysical Research: Space Physics*, *123*, 287–296. https://doi.org/10.1002/2017JA024536

Tenishev, V., Combi, M. R., Teolis, B. D., & Waite, J. H. (2010). An approach to numerical simulation of the gas distribution in the atmosphere of Enceladus. *Journal of Geophysical Research*, *115*, A09302. https://doi.org/10.1029/2009JA015223

Tenishev, V., Öztürk, D. C. S., Combi, M. R., Rubin, M., Waite, J. H., & Perry, M. (2014). Effect of the Tiger Stripes on the water vapor distribution in Enceladus' exosphere. *Journal of Geophysical Research: Planets*, *119*, 2658–2667. https://doi.org/10.1002/2014JE004700

Teolis, B. D., Perry, M. E., Hansen, C. J., Waite, J. H., Porco, C. C., Spencer, J. R., & Howett, C. J. A. (2017). Enceladus plume structure and time variability: Comparison of Cassini observations. *Astrobiology*, *17*(9), 926–940. https://doi.org/10.1089/ast.2017.1647

Teolis, B. D., Perry, M. E., Magee, B. A., Westlake, J., & Waite, J. H. (2010). Detection and measurement of ice grains and gas distribution in the Enceladus plume by Cassini's ion neutral mass spectrometer. *Journal of Geophysical Research*, *115*, A09222. https://doi.org/10.1029/2009JA015192

Thissen, R., Witasse, O., Dutuit, O., Wedlund, C. S., Gronoff, G., & Lilensten, J. (2011). Doubly-charged ions in the planetary ionospheres: A review. *Physical Chemistry Chemical Physics (Incorporating Faraday Transactions)*, *13*, 18264. https://doi.org/10.1039/C1CP21957J

Tokar, R. L., Johnson, R. E., Thomsen, M. F., Wilson, R. J., Young, D. T., Crary, F. J., et al. (2009). Cassini detection of Enceladus' cold water-group plume ionosphere. *Geophysical Research Letters*, *36*, L13203. https://doi.org/10.1029/2009GL038923

Waite, J. H., Glein, C. R., Perryman, R. S., Teolis, B. D., Magee, B. A., Miller, G., et al. (2017). Cassini finds molecular hydrogen in the Enceladus plume: Evidence for hydrothermal processes. *Science*, *356*(6334), 155–159. https://doi.org/10.1126/science.aai8703

Waite, J. H., Glein, C., Postberg, F., & Lunine, J. (2019). Enceladus as revealed by the Cassini-Huygens mission. In *Lunar and Planetary Science Conference* (pp. 1290).

Waite, J. H., Lewis, W. S., Magee, B. A., Lunine, J. I., McKinnon, W. B., Glein, C. R., et al. (2009). Liquid water on Enceladus from observations of ammonia and ^{40}Ar in the plume. *Nature*, *460*, 487–490. https://doi.org/10.1038/nature08153

Wellbrock, A., Coates, A. J., Jones, G. H., Lewis, G. R., & Waite, J. H. (2013). Cassini CAPS-ELS observations of negative ions in Titan's ionosphere: Trends of density with altitude. *Geophysical Research Letters*, *40*, 4481–4485. https://doi.org/10.1002/grl.50751

Westlake, J. H., Waite Jr., J. H., Carrasco, N., Richard, M., & Cravens, T. (2014). The role of ion-molecule reactions in the growth of heavy ions in Titan's ionosphere. *Journal of Geophysical Research: Space Physics*, *119*, 5951–5963. https://doi.org/10.1002/2014JA020208

Yeoh, S. K., Li, Z., Goldstein, D. B., Varghese, P. L., Levin, D. A., & Trafton, L. M. (2017). Constraining the Enceladus plume using numerical simulation and Cassini data. *Icarus*, *281*, 357–378. https://doi.org/10.1016/j.icarus.2016.08.028

Young, D. T., Berthelier, J. J., Blanc, M., Burch, J. L., Coates, A. J., Goldstein, R., et al. (2004). Cassini Plasma Spectrometer investigation. *Space Science Reviews*, *114*(1), 1–112. https://doi.org/10.1007/s11214-004-1406-4